Accessing radiation damage to biomolecules on the nanoscale by particle-scattering simulations

Journal of Physics Communications

TOPICAL REVIEW

Accessing radiation damage to biomolecules on the nanoscale by particle-scattering simulations

Marc Benjamin Hahn

Bundesanstalt für Materialforschung und Prüfung, 12205 Berlin, Germany

E-mail: marc-benjamin.hahn@fu-berlin.de

Keywords: radiation damage, Geant4, Geant4-DNA, TOPAS, TOPAS-nBio, microdosimetry, particle scattering simulations

OPEN ACCESS

RECEIVED
2 January 2023

REVISED
10 March 2023

ACCEPTED FOR PUBLICATION
6 April 2023

PUBLISHED
17 April 2023

Abstract

Radiation damage to DNA plays a central role in radiation therapy to cure cancer. The physico-chemical and biological processes involved encompass huge time and spatial scales. To obtain a comprehensive understanding on the nano and the macro scale is a very challenging tasks for experimental techniques alone. Therefore particle-scattering simulations are often applied to complement measurements and aide their interpretation, to help in the planning of experiments, to predict their outcome and to test damage models. In the last years, powerful multipurpose particle-scattering framework based on the Monte-Carlo simulation (MCS) method, such as *Geant4* and *Geant4-DNA*, were extended by user friendly interfaces such as *TOPAS* and *TOPAS-nBio*. This shifts their applicability from the realm of dedicated specialists to a broader range of scientists. In the present review we aim to give an overview over MCS based approaches to understand radiation interaction on a broad scale, ranging from cancerous tissue, cells and their organelles including the nucleus, mitochondria and membranes, over radiosensitizer such as metallic nanoparticles, and water with additional radical scavenger, down to isolated biomolecules in the form of DNA, RNA, proteins and DNA-protein complexes. Hereby the degradation of biomolecules by direct damage from inelastic scattering processes during the physical stage, and the indirect damage caused by radicals during the chemical stage as well as some parts of the early biological response is covered. Due to their high abundance the action of hydroxyl radicals ($^{\bullet}$OH) and secondary low energy electrons (LEE) as well as prehydrated electrons are covered in additional detail. Applications in the prediction of DNA damage, DNA repair processes, cell survival and apoptosis, influence of radiosensitizer on the dose distribution within cells and their organelles, the study of linear energy transfer (LET), the relative biological effectiveness (RBE), ion beam cancer therapy, microbeam radiation therapy (MRT), the FLASH effect, and the radiation induced bystander effect are reviewed.

1. Introduction

Exposure to high-energy radiation occurs during radiation therapy for cancer treatment, medical imaging, or long-term space flights. Hereby the radiation damage to biological tissue can be described from two conceptual diametrical points of view. From the macroscopic point of view, the damage in irradiated tissue depends on type of the cells, the radiation properties and the corresponding dose [1]. On the nanoscale, the damage to individual biomolecules is of concern, which is directly related to inelastic scattering events and the radical chemistry involved. To advance radiation therapy and to provide optimal radiation protection, a comprehensive understanding of the mechanisms encompassing macroscopic dose-deposit and cell-survival, as well as degradation of biomolecules upon ionization and radical attack, has to be achieved. However, the physical, chemical and biological processes involved, cover a broad spatial-range (from Å to cm, figure 1), time-scale ($10^{-16}\ s - 10^{3}\ s$, figure 2) and complexity, spanning from isolated molecular building-blocks of life to the response of ensembles of cells to external stress [2].

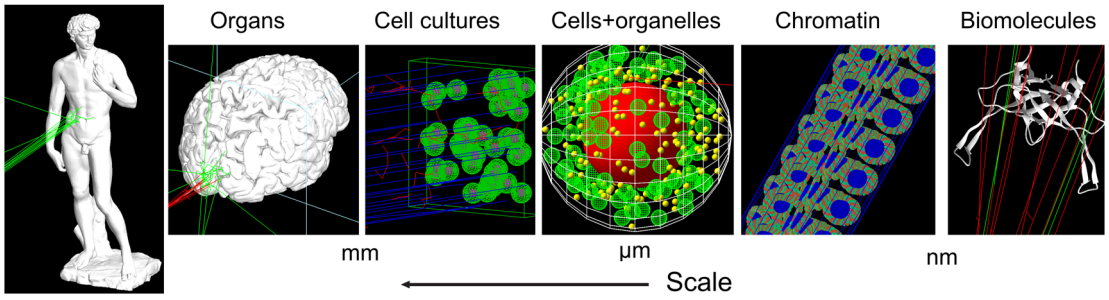

Figure 1. Simulation of irradiations from the macro to the nano scale, from left to right: Photon irradiated David by Michelangelo [13], electron irradiated human brain [14], proton irradiated cell culture [15], cell model with organelles and nanoparticles as radiosensitizer [16], Chromatin model [15, 17], and a electron irradiated single-stand DNA-binding protein G5P [18]. Simulations and images were generated by TOPAS [19] and are based on either STL models, files or geometries included in TOPAS-nBio [15].

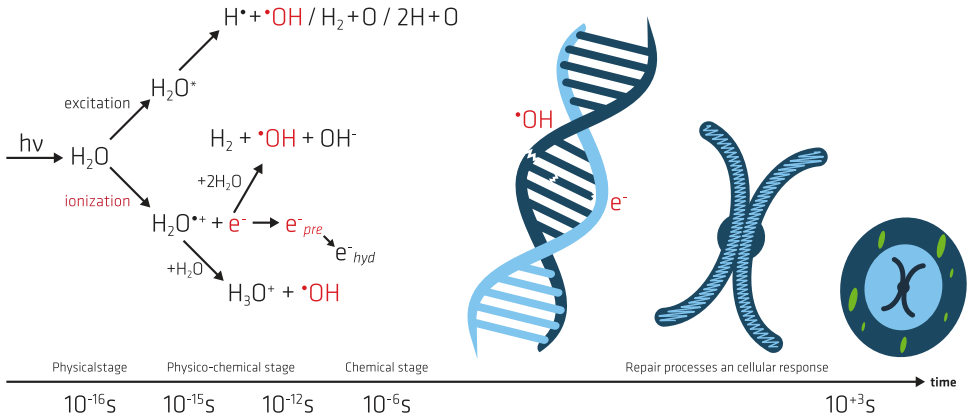

Figure 2. The different stages of radiation interaction with water (physical stage), the intermediate states (physico-chemical stage) and subsequent reaction, diffusion (chemical stage) upon water radiolysis. Resulting in DNA damage (center) and possible repair processes in the cell over a wide time scale. Timescales are approximate and sizes are not to scale. Image based on [3]. For details see the text.

1.1. Why particle scattering simulations?

To investigate the ultrafast scattering processes on the atomic scale in the sub-femtosecond range, the radical production, and diffusion over nanometer distances within pico to nanoseconds, and the biological damage response and repair processes which take place in a timespan of seconds to hours simultaneously (figure 2), a broad range of experimental techniques and scientific disciplines are required [3]. To further combine and unify the resulting radiation-effect models describing these phenomena, which are developed by interdisciplinary research activities throughout biophysics, radiation biology and medicine, a multi-scale approach has to be developed [2]. Here, the combination of computer simulations with experimental results allows to bridge these scales in unifying models by predicting parameters which are difficult to access by experimental methods alone [4]. For instance, to connect the microscopic scattering events of high-energy particles at chromosomes in a cell nucleus, with the macroscopic coefficients used to describe cell-survival models, various events have to be considered: The energy deposit throughout the irradiated tissue, the microscopic damage-event at the DNA molecule within the nucleus, the decay channels and radical transfer processes within DNA, following the initial damage event, and the cellular repair response and pathways which can lead to survival, mutation or cell death [2].

Before reviewing the work related to this effort, the differences between macroscopic dosimetry, microdosimetry and nanodosimetry, have to be introduced briefly. Further details of the application of related methods, their limitations and possible extensions were published by various authors throughout the last years [1, 2, 5–12].

1.2. Macroscopic and microscopic image

When radiation interaction with complex biological systems, such as human beings or cell colonies, is described in terms of 'classical' dosimetry, the involved microscopic reactions are not analyzed in detail. Here, a certain biological outcome (e.g. cell death) is expressed in terms of macroscopic quantities such as the absorbed,

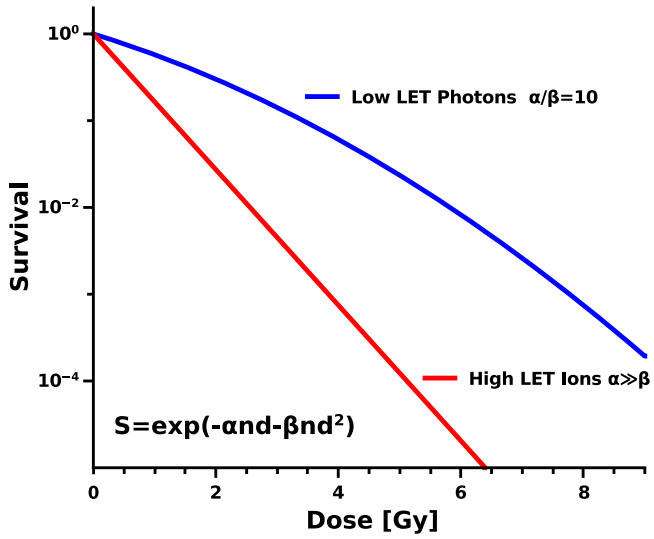

Figure 3. Sketch of cell survival in dependence of the dose as predicted by the linear-quadratic (LQ) model for low LET photons (blue) and high LET ions (red). For details see the text.

equivalent or effective dose [7]. The fundamental, physical quantity of dosimetry is the absorbed dose (D) in tissue given in Gray (1 Gy = 1 J/kg) [20]. However, the probability of a biological effect depends not only on the absorbed dose alone, but also on the type and energy of the radiation and the irradiated tissue. Thereby the type of radiation and kinetic energy influence the spatial distribution, density, and energy spectrum of the secondary electrons (δ-rays) produced along its trajectory [1, 7]. These radiation and tissue specific effects are considered phenomenologically by radiation and tissue weighting factors. The factors are set by the *International Commission on Radiation Units and Measurements* (ICRU) and the *International Commission on Radiological Protection* (ICRP). Hereby, the ICRU is responsible for establishing the units and definitions used in dosimetry and medical physics, while the ICRP issues recommendations for the medical application and radiation protection [1]. These weighting factors are related to clinical cell survival curves or other biological effects (BE) in dependence of irradiation [21]. The radiation induced BE can be expressed by the empirically determined linear-quadratic equation as

$$BE = \alpha D + \beta D^2, \tag{1}$$

with D as the absorbed dose, and α and β corresponding to the initial and final slopes of survival curve of irradiated cells (figure 3) [22]. The parameters α and β are therefore related to the radiosensitivity of the cell, whereby they can be interpreted such, that α represents cell death or a BE from single-hit events, while β represents the effects from multiple-hits [23]. Furthermore, the relation is assumed to be valid in dose range between 2-10Gy [21].

For details on the different weighting factors and their relation to BE, and the change of the recommendations with time, compare the literature [1, 20] and references therein. Despite the success of this macroscopic description in medicine and radiation protection, it is far from being complete. This is due to the fact, that one averaged macroscopically registered dose, can be the result of various microscopic chain of events, resulting in different BE values as given in equation (1). Radiation which produces ionization events which lie in the range of the distances between the base pairs of DNA are more effective in damaging DNA substantially, and therefore lead for the same dose to a higher BE. To compare the effects of different types of radiation the term relative biological effectiveness (RBE) was introduced, which describes the ratio of two different absorbed doses of different radiation to cause the same BE. Furthermore, the same dose can be deposited in a cell either by many scattering events evenly distributed over the whole cytosol, or very localized, within the nucleus of a cell. Hereby, the latter can be assumed to lead to cell death with a much higher probability than the former. Thus, the stochastic nature of elementary scattering processes, as well as the effects of different particle trajectories, and the variation of energy deposit along the trajectory, have to be considered to obtain a complete picture. Since these nanoscopic properties are very difficult to access by experiments alone, simulational techniques and different descriptions of 'dose' and events on the microscale and nanoscale were developed to bridge that gap. This is often described by the terms microdosimetry and nanodosimetry [5,7,8,24–26].

1.3. Bridging the gap between the micro and macro world

For example, micro and nanodosimetric simulations can be performed to determine track structures of particles and their interactions and energy deposit within a target molecule, such as DNA, and the frequency of their occurrence. In a second step the damage at different sites of DNA can be predicted and its complexity being determined. Here, the term complex damage refers to closely located lesions in DNA, which are difficult to repair [27, 28]. By such an approach one aims to connect the microscopic physical and chemical processes to predict experimental outcome. This involves the mechanistic description of the scattering processes by atomic and molecular physics, the chemical reactions, and the abstraction of the damage models by means of the target theory, as well as a possible inclusion of biological repair mechanisms [29]. Due to the complex nature of the problem, many simplifications have to be made during the modelling of the processes on the different scales. This review aims to give an overview over the different experimental and computational approaches and their combination to bridge between these scales. It is structured as follows: In section 2 a brief overview over functions and features of particle-scattering simulation and available packages is given. In the following sections different aspects of radiation damage in biological tissue, and the involved mechanisms are discussed. Hereby section 3 presents the different types of high-energy radiation used in radiation therapy, and the secondary particles produced during the early stage of radiation-matter interaction, in the so called physical-stage. This is followed by a subsection about the radicals produced upon water radiolysis during the physico-chemical stage and their diffusion and reaction behavior in the chemical-stage. Section 4 focuses on the targets of radiation therapy and how they are investigated on the various scales by simulational methods in combination with different irradiation setups, as well as related analytical tools. Hereby, the range of individual molecules to whole cells, including radiosensitizers are covered. Emphasis is also placed on studies that go beyond the purely descriptive approach and aim to predict the outcomes of irradiation experiments and bridge the gap between the microscopic and macroscopic description of radiation effects on biological targets. The final section 5 gives an outlook about topics which will become increasingly relevant in the future and will require new approaches in modelling the interplay in complex structures.

2. Simulations to the rescue

The understand the capabilities and limitations of particle-scattering simulations a brief overview over their function and features is given.

2.1. Simulation codes

A broad variety of simulation toolkits for studying particle-matter interaction exist, some of the codes and their extensions applied in the field of radiation biophysics are PARTRAC [8, 30], FLUKA [31], MNCP [31], KURBUC [32], MBN-explorer [33], Geant4 [34, 35] Geant4-DNA [36, 37], TOPAS [19], and TOPAS-nBio [15]. They differ in their capabilities and focus in terms of available particles, energy ranges, target models and user interfaces, details can be found in the literature given above and references therein. In this review the focus lies on studies performed with the particle-scattering framework *Geant4* [34, 35] and *Geant4-DNA* [36, 37], which is based on the Monte-Carlo method, and their user friendly interfaces provided by *TOPAS* [19] and *TOPAS-nBio* [15]. This selection was made since these frameworks are under active development, freely available to the scientific community, have a very broad scope with respect to energy range, simulated particles and targets [38], they are easily extendable, provide high flexibility which allow for simulation of the physical [37] and chemical stage [39, 40], DNA repair processes [17, 41], microdosimetric calculations [42, 43], cells and nanoparticles [16], as well as inclusion of *computer aided design* (CAD) geometries [44] and molecular structures by custom models [45] or via the format of the *protein database* (PDB) [46].

2.2. Geant4 and Geant4-DNA

Geant4 (*GEometry ANd Tracking*) is a general-purpose Monte-Carlo simulation (MCS) toolkit which was originally developed for high-energy, nuclear and accelerator physics at CERN [34, 35]. It provides functionality to calculate the passage of particles through matter from some eV to the TeV range. Geant4 is implemented in C ++ and offers low-level features to obtain tracking, hits and interaction information, to define complex geometries and adjust physics models in a flexible manner. It covers electromagnetic, hadronic and optical processes for a broad range of particles, including photons, electrons, positrons, protons, neutrons, and various ions. Geant4 allows to perform quick calculations by applying condensed-history or detailed track-structure simulations for increased spatial accuracy. Details about the underlying physics and related calculation methods can be found in the *Physics Reference Manual* provided by the Geant4 collaboration [47]. Geant4-DNA [36, 37] extends Geant4 by adding track-structure modeling with optimized discrete scattering cross-sections for electrons, protons, selected atoms and ions for liquid water which increases the accuracy on the nanometer scale

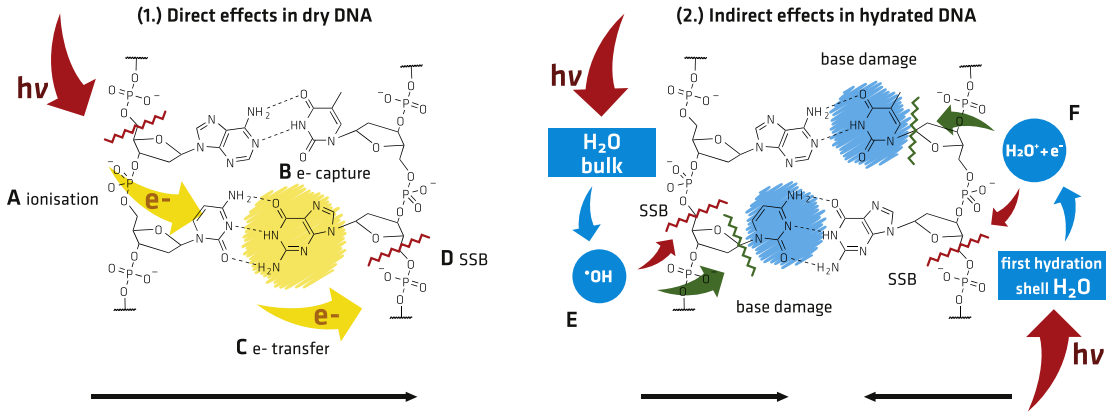

Figure 4. Example of (1.) direct and (2.) indirect radiation damage in double-stranded DNA. Direct effects (1.) can produce SSB (red lines) by ionization events (A) of DNA (red arrows), or secondary low-energy electrons via the formation of transient negative ions the nucleobases (B), and subsequent electron transfer (C) and rupture of a C-O bond (D) in the DNA backbone. Quasi-direct (2. F) and indirect damage (2. E) involves ionization of water molecules in the bulk (E) or in the first hydration (F) layer representing the most important processes. Green lines represent base damage and loss. Taken with permission from [56].

[37, 48]. During the last years extensive effort was undertaken to validate the scattering models against previously validated simulation codes and experimental data [35] for applications in space-radiation environment [49], radioactive decay [50], and particle scattering at liquid water [36], and data sets from the ICRU reports [51]. Furthermore, simulation of radical production and their diffusion during the physico-chemical and chemical stage were implemented in Geant4 by the Geant4-DNA collaboration [36, 37] and were described in detail by Karamitros *et al* [39, 52]. The flexibility of Geant4 allows users to adapt the provided scattering models, tracking and scoring to their problem. However, this needs expert knowledge to understand the interplay of the different components and to implement proper *C++* code describing the problem.

2.3. TOPAS and TOPAS-nBio

To overcome this complication the TOPAS (*TOol for PArticle Simulation*) interface was developed, which primary goal was to provide a user-friendly tool for research and clinical physicists with a focus on proton therapy [19]. TOPAS provides an easier way than pure Geant4 to define complete experiments in easy to read text files, adds additional scorers and features such as changing the simulation geometry over time [19]. TOPAS-nBio wraps and extends the features of Geant4-DNA and makes additional microscopic geometries [15], such as DNA [53], cells [45], cells with nanoparticles [16], and simulations of chemical processes [54], and combinations thereof available by ready to use examples. Various applications on different scales will be discussed in the following sections.

3. The physical and chemical stage of radiation damage

To understand the diverse processes leading to various types of damage in biological tissue, they can be classified in dependence of the involved species, mechanisms and outcome. For example, when an incoming particle undergoes an inelastic scattering process directly at a biomolecule (figure 4), resulting modifications are classified as direct damage [3, 55, 56]. In contrast, indirect damage is related to ionization of the solvent or cosolutes and the production of radicals, such as reactive oxygen species (ROS), which react with the target. Hereby water plays a major role due to its abundance in biological tissue. For instance, human cells consist of more than 70 % water [3]. Therefore, a large amount of the energy of ionizing radiation is transferred to water by inelastic scattering processes, instead of being directly deposited within biomolecules. The subsequent radiolysis of water molecules leads to the production of secondary particles such as electrons and radicals. These interactions and the following processes occur on time scales between $10^{-15} - 10^{-6}$ s [3, 57]. They can be classified according to their sequence and the additional reactions, as sketched in figure 2. Within the *physical stage*, which takes place within less than 10^{-15} s, the inelastic scattering processes between the incident high-energy radiation and either biomolecules, or water occur. The following physico-chemical stage $(10^{-15} - 10^{-12})$s describes intra-molecular and inter-molecular energy transfer after excitation [3]. If a short lived water cation in the first hydration shell of a biomolecule is produced, electron transfer (ET) reactions can occur directly between the cation and the biomolecule without additional intermediate states. According to the classification scheme introduced by Becker and Sevilla [58], this damage can be categorized as quasi-direct, and

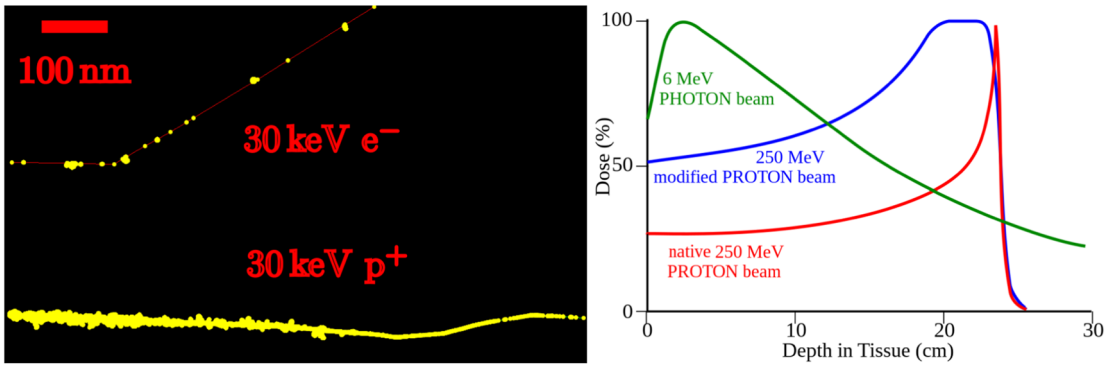

Figure 5. Left: 30 keV electron (top) and proton (bottom) track in liquid water (red) and the location of ionization events (yellow) simulated with Geant4-DNA. Right: Normalized depth-dose curve of MeV photons (green), native protons (red) and modified proton beams (blue).

is thought to be of high-importance for the formation of DNA double strand breaks (DSB) [55, 59, 60]. Ionization of bulk water molecules can lead to their radiolysis via various pathways (figure 2) [57, 61, 62]. The diffusion, recombination, and subsequent chemical reactions of the radiolysis products are completed within $(10^{-12} - 10^{-6})$s. This period is called the chemical stage.

The overall relation, mechanisms and quantitative contributions from direct, quasi-direct, and indirect damage are still controversially debated, despite the fact that they were investigated intensively during the last decades [56,62–69]. This is mostly owed to the experimental difficulties to clearly separate the effects and mechanisms from each other. Because the occurrence of quasi-direct and indirect damage depends on the presence of water, to produce either water cations in the first hydration shell, or ROS in the bulk. On the other hand, direct effects do not depend on water directly, however the interaction and energy transfer mechanisms with and within biomolecules might be modified by its presence. This was suggested by simulations on nucleotides, and experimental work on tetrahydrofuran (THF), there solvation showed a strong influence on damage induction [70–72]. Details on these questions and and their investigation by experiment and simulations are described in the following.

3.1. Physical stage and inelastic scattering

High-energy photons, electrons, nucleons and ions differ strongly in their scattering behaviour and spatial energy deposit distribution in dependence of their kinetic energy. However, they all have in common that they can cause breakage of molecular bonds or formation of cationic radicals after an ionization event. The detailed outcome of such events depends on many factors. For example, the type of molecule, the initial location of the ionization event, and the chemical environment play important roles. The following sections will focus on general mechanisms and water related effects. A detailed discussion on radiation damage to DNA and proteins is given afterwards in section 4.

3.1.1. High-energy particles

Most primary particles used in radiation therapy have initial energies in the MeV range. At these energies photons interact with matter by processes such as Rayleigh scattering, the photo-electric effect, Compton-scattering, Auger effect, or pair-production [57]. The former scattering events produce additional electrons, while pair production results in the creation of an electron-positron pair when the kinetic energy is above the threshold of 1.022 MeV. For high-energy electrons (HEE) elastic scattering determines their track structure while inelastic scattering by ionization or creation of Bremsstrahlung determines the energy deposit. The energy loss of HEE in medium can described by a general formalism, via the Bethe theory and dielectric-response function as a function of energy and momentum transfer [48, 73]. In contrast to charged particles, neutrons collide mostly with the nucleus of atoms or can be captured by them. Heavy charged particles such as protons and ions can interact with the electron clouds or with the nuclei of the atoms of the medium, leading to ionizations, charge transfer or collisions [2]. Furthermore, their scattering cross section increases strongly at low kinetic energies, leading to a strong increase of the energy deposit at the end of the track. This region of a dose-depth curve is called the Bragg peak (figure 5 right, red curve). By modifying the initial energy of these heavy high-energy particles by an attenuator, the depth of that region can increased in depth, resulting in the so called spread out Bragg peak (SOBP) as shown in figure 5 right, blue curve. This allows for precise irradiation of tumors. To make use of the appearance of this highly localized energy deposit, ion beam cancer therapy (IBCT) was developed. To optimize the biological effectiveness of IBCT simulation and modelling techniques are

frequently applied [74–76]. Details on related simulations with optimized parameter sets can be found in the work by Velten and Tomé [77]. Recently, the proton scattering models were extended to cover the whole energy range of proton radiotherapy up to 300 MeV [78]. To understand the properties of energy depositions in subcellular-sized volumes these heavy particles are investigated by MCS and their microdosimetric properties are determined [79]. Similarly, dose distributions for microbeam radiation therapy (MRT), which allows for precise targeting of cancerous tissue, were studied by Geant4 based MCS and evaluated for different types of radiation, or against other MCS codes, such as Penelope [80–82]. Overall, a combined experimental and simulational effort was undertaken to validate cross section data and scattering within the last years as described by various authors for the different types of primary particles in detail [51,83–87].

3.1.2. Linear-energy transfer and mean lineal energy

A variety of microdosimetric quantities are used to classify radiation effects in one and three dimensions. This is necessary since high-energy particles can differ substantially in their energy deposit characteristic (figure 5 left). In one dimension the energy deposit characteristics are described in a simplified manner by the *linear energy transfer* (LET). It is defined as the energy deposit per unit length in a given medium. Radiation is often denoted as either low LET (e.g. ^{60}Co γ-rays: 0.2 $keV/\mu m$) and high LET (>10 $keV/\mu m$) [88]. radiation. Furthermore, different particles can have similar LET when differing in kinetic energy. For example, γ particles from ^{60}Co with 1.3 MeV and ^{137}Cs with 0.5 MeV kinetic energy, or HEE in the range of (1-10)MeV, have a very similar LET (<1 $keV/\mu m$) [57, 62]. A more complex quantity which was defined to incorporate three dimensional and stochastic effects of radiation is the lineal energy, which is, in contrast to the LET, a directly measurable quantity, as discussed in detail by Lindborg *et al* [21]. Lineal energy is defined as the energy deposited in matter in a given volume by a single energy deposition event, and should be applied for dosimetric analysis in subcellular volumes with characteristic length below 100 nm [21]. Extensive collections of microdosimetric parameter for particles such as x-rays, electrons [89] and ions can be found in the monographs of published by the Karolinska institute as listed by Nikjoo *et al* [90]. Examples and extensions to calculate microdosimetric quantities with Geant4 and TOPAS are described by Ivanchenko *et al* [91] and Zhu *et al* [92], respectively. The energy transferred to the medium from the high-energy particles during inelastic scattering events leads to the production of secondary electrons along their track [3]. Per MeV deposited energy about 5×10^4 secondary electrons (SEs) are produced [65]. The high abundance of SEs produced by the primary particles makes them one of the main sources of direct damage at biomolecules.

3.1.3. Many faces of secondary electrons in water

The high-energy SEs produced along radiation tracks are called δ-rays. They release their energy to small volumes around the trajectory of the initial high-energy particle. When a trajectory of such a δ-ray is within nanometer distance of a biomolecule, complex damage becomes likely due to the high local density of scattering events it produces. Experimentally, the electron trajectories on the nanoscale are difficult to access. In addition to analytical approaches, Monte Carlo methods have been used to determine the spatial energy deposit distribution in the vicinity of biomolecules successfully[3]. The interaction of the resulting non-thermal SEs with matter depends strongly on their kinetic energy. Thus, their initial kinetic energy spectrum and spatial distribution are of uttermost importance to understand radiation damage and predict the outcome. These properties were investigated intensively by La Verne, Pimblott and coworkers via MCS [93–97]. They determined the dipole oscillator strength distribution for water and solid, dry DNA from experimental data to predict electron stopping power, the mean-free path, the inelastic cross-section and the distribution of energy-loss events for electrons with kinetic energies between 5 keV and 1 MeV [93, 95]. The dipole oscillator strength distribution peaks between 18-20 MeV in liquid water, and at about 24 eV in dry DNA [95]. Plasmon excitations in liquid water were estimated to be absent [94]. For 1MeV the most probable energy loss in dry DNA and liquid water calculated as 23 eV. The mean energy loss in dry DNA and liquid water was determined as 57.9 eV and 56.8 eV, respectively. The mean excitation energy of dry DNA was shown to be 77.9 eV and for liquid water 74.9 eV [93, 95]. The secondary electrons spectra produced by protons and helium ions with kinetic energies in the MeV range was studied by the same authors [97]. They determined the most probable energy of secondary electrons being around 9 eV and the mean energy for secondary electrons being in the range of 50 eV to 60 eV. Furthermore, Nikjoo *et al* studied the mean number of inelastic interactions, ionization events and energy deposit of electrons with energies between 100 eV to 4500eV and the resulting DNA damage of different complexity in combination with a cylindrical DNA model and generated extensive datasets on strand-break induction in DNA [32]. This was later on extended to electron energies up to 100keV with a focus on damage prediction and comparison with experimental data [98]. Similarly the energy spectra and energy deposit characteristics of Auger electrons emitted from the radionuclides ^{124}I and ^{124}I in water vapor and the liquid phase were determined [99].

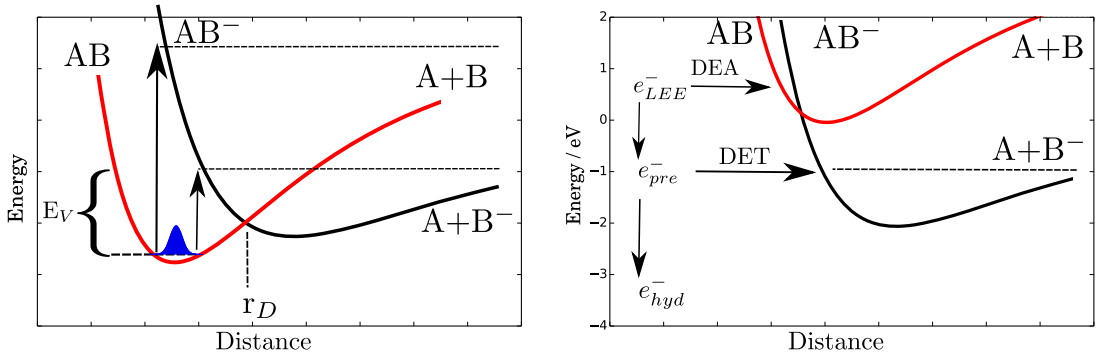

Figure 6. Shown are the potential energy in dependence of the distances of the neutral (red) and negatively charged molecules (black). **Left:** Shown is Dissociative electron attachment (DEA) and the transition from the neutral ground state to the excited within the blue Franck-Condon region. E_V is the vertical excitation energy which can lead to dissociation. r_D represents the intersection of both potential curves. **Right:** Comparison between DEA and Dissociative electron transfer (DET) together with the corresponding states of the free (kinetic) electrons (e^-_{LEE}), the presolvated electron (e^-_{pre}), and the fully hydrated electron (e^-_{hyd}). Image taken with permisson from [108] and originally adapted from [109–111].

Independently of the SEs initial kinetic energy they will undergo subsequent scattering processes, loose energy and become eventually low-energy electrons (LEE) with kinetic energies below 100 eV. For LEEs with kinetic energies down to 20 eV the dominant inelastic scattering processes in water is still ionization [3, 100]. Here, the production of a unbound electron by ionization of water molecules requires at least (11.7± 0.2)eV [101]. Below 20 eV, kinetic energy electronic excitation and electron attachment contribute increasingly to the radiolysis of water [3, 100]. These electrons with kinetic energies below 20 eV are sometimes called very low energy electrons (vLEEs) [102]. Their penetration depth for kinetic energies between 7-20 eV in liquid water around 298 K varies between (8.8-20)nm [103, 104]. Furthermore, at that energy additional inelastic processes become relevant. Between 6.5 eV and 9.3 eV excitation energy [101, 105, 106] electron transfer (ET) from H_2O can produce excited, short-lived intermediate states of the so called prehydrated or presolvated electron (e^-_{pre}) with lifetimes between 100 fs-500 fs (compare figure 6 right) [101, 105, 107]. In the range of 8 eV-11 eV these processes compete against each other [101]. Electron attachment to water molecules is particularly relevant at kinetic energies up to 9 eV. It can lead to the formation of unstable transient negative ions (TNI) and subsequent dissociation of water molecules (figure 2 left) [3]. Measurements on ice showed that mainly H^- and $^{\bullet}OH$ are formed from the dissociation of such TNI [3]. The vLEEs become even more important when one considers that they do not only interact with water alone, but can damage DNA as well, even when their kinetic energies are below the ionization threshold [63]. This happens similarly to the processes in water: beginning with the formation of TNIs, possible intermolecular electron transfer, and subsequent dissociative electron attachment (DEA) as sketched in figure 6 left, or by core-excited resonances for electrons with kinetic energies above 4 eV [63, 65, 112].

When a vLEE looses all kinetic energy, it leaves the conduction band of water and can reside in a presolvated state for about 200 fs-500 fs (figure 6 right), similar to the electron being ejected directly from a water molecule as described above [113]. In this state it is delocalized over about 4 nm [114] and weakly bound to the environment with potential energies of about −1.0 eV to −1.5 eV [113]. Then, reorientation of the surrounding water molecules leads to the formation of a hydrated, more stable and localized (ca. 2.5-3Å), bound state (-3.2 eV) with an s-wave function (figure 6 right) [107, 114].

To perform reliable MCS of these low-energy processes accurate cross sections are needed. Due to the short inelastic mean free path (IMFP) of LEE at ambient pressure in water, which is of the order of nanometers, and the ultra-high vacuum (UHV) environment required for electron-energy loss spectroscopy (EELS), the available cross sections are based on extrapolated values from amorphous ice measured by Michaud, Sanche and coworkers [115–117]. These specialised cross sections for scattering of LEE at water were introduced into Geant4-DNA and TOPAS-nBio by the *G4Water* material and related list of physics models, *G4DNA*. Here, specialised scattering models for electrons for elastic scattering, ionisation, electron attachment, vibrational excitation, and emission of Bremsstrahlung are provided. Extensive work was carried out to validate them against previous implementations in other MCS code and experimental datasets [51, 83, 85, 87]. Further details about the production, properties and fate of LEE and vLEEs in water can be found in the review by Alizadeh and Sanche [3].

3.2. Chemical stage: Indirect damage

Indirect damage at biomolecules is caused by chemical reactions with radicals originating from radiation interaction with water or cosolutes. Depending on the presence of cosolutes, pH, amount of oxygen and other parameters a huge variety of pathways, different reactive oxygen species (ROS) and organic radicals have to be considered [69]. Here the focus lies on the most important species which are implemented in Geant4-DNA and TOPAS-nBio. Examples of the products of ionization and excitation processes together with their subsequent reaction pathways are depicted in figure 2. For a complete overview over the other species the reader is referred to the classical textbooks by von Sonntag [61, 62].

3.2.1. Radical production and diffusion

At keV energies, the radiolysis of water is dominated by ionization events. The production of H_2O^+, hydroxyl radicals ($^{\bullet}OH$) and secondary electrons (e^-) after ionization of water molecules can be described by the net-ionization reaction:[56, 118]

$$\gamma + 2\,H_2O \rightarrow H_2O^+ + e^- + H_2O \rightarrow H_3O^+ + ^{\bullet}OH + e^- \tag{2}$$

The intermediate H_2O^+ cation, as precursor of the hydroxyl radical, is of special importance in this process (figure 2 left). Due to its structural similarities to the normal water molecule some authors assume the possibility of rapid migration of the H_2O^+ cation [119]. The migration distance of H_2O^+ and its reaction products is required for modelling the chemical stage in MCS, and to determine their interaction probability with biomolecules in their vicinity. The average range of the different diffusing species is in the nanometer range. The prehydrated electron with a lifetime of a few hundred femtoseconds is delocalized over a range of up to 4nm [114]. Hereby the exact extension of the wave function of the prehydrated electron depends on its generation and history as well as on the assumed state (e.g. excited in the p-orbital, Rydberg state, influence of interfaces) [107, 111, 114, 120]. The values for the diffusion range of the $^{\bullet}OH$ radical are in the range of 2-7nm and are determined by its diffusion constant of about $D_{^{\bullet}OH} = 2.8\ nm^2s^{-1}$ and the reaction probability with the surrounding medium [118, 121, 122]. In Geant4-DNA the production of hydroxyl radicals upon ionization or excitation of water molecules can be simulated [52]. Hereby different decay channels for the various excitation states are considered. Leading to the production of various species and their diffusion (standard diffusion constant given in brackets as $10^{-9}\ m^2s^{-1}$) can be simulated e^-_{hyd} (4.9), $^{\bullet}OH$ (2.8), $H^{\bullet}$ (7.0), H_3O^+ (9.0), H_2 (4.8), ^{-}OH (5.0) and H_2O_2 (2.3). A detailed summary of all reactions, G-values and the implementation in a step-by-step approach as well as comparison between Geant4-DNA and PARTRAC is provided in the literature [39, 52, 118]. An additional approach based on the independent reaction times (IRT) model, which facilitates the simulation of the reactions of spatially inhomogeneous distributions of large numbers of particles, is provided in Geant4-DNA and TOPAS-nBio to speed these calculations up [123–125]. Further details on the underlying reaction mechanism and additional detailed datasets on molecular excitations, dissociation schemes, reaction, and diffusion parameters during the chemical stage can be found in additional literature and references therein [118, 126]. TOPAS-nBio allows for simulation of an extended list of chemical species such as O_2 (2.4), O_2^- (1.75), HO_2 (2.3) and HO_2^- (1.4) [40]. These models were successfully applied to predict temperature dependent DNA strand-break yields in plasmid DNA [127]. However, in general it has to be noted, that the simulation of the chemical stage with extended time scales up to the microseconds and short time steps is comparatively slower than the simulation of the scattering processes during the physical stage. Therefore, besides applying the IRT models, extended computational resources are needed when extended set of histories shall be studied during the chemical stage. Furthermore, TOPAS-nBio was recently extended to allow for the simulation of intertrack reactions between reactive species produced during different simulation tracks [128].

This feature is of special importance for new therapeutical approaches which make use of the FLASH effect to decrease the radiation toxicity while achieving the same tumor control [129, 130]. Hereby dose rates above 40 Gy/s are applied, which are beyond the conventional dose rates of (0.5-20) Gy/s, leading to the possibility of intertrack reactions during the chemical stage and the possibility of altered biological response [129]. Various hypotheses have been put forward to explain the reduced radiation sensitivity in normal tissue by the FLASH effect [129–132]. The hypotheses based on 'chemical models' are having in common, that they consider a complex interplay of LET, oxygen content, the modification of the oxygen enhancement ratio (OER), as well as intra and intertrack recombination of various radical species. Hereby, the OER describes the different radiosensitivity of cells under aerobic and and hypoxic conditions, which decreases normally with increasing LET of the radiation [133]. These processes and their interplay are currently controversially debated and topic of ongoing research [129, 130, 132]. The first hypothesis assumes transient 'radiolytic oxygen depletion' (ROD) due to radiation induced oxygen consumption [129, 130, 134]. Hereby, the high dose rates consume the oxygen so quickly that the cellular dose-response curves are showing the characteristics of hypoxic conditions, i.e. increasing the radiation resistance of healthy tissue [134]. In contrast, the 'oxygen in track' hypothesis proposes a radiation induced oxygen production within the track of high LET radiation. Accordingly, MCS were performed by Meesungnoen and Jay-Gerin to study the formation of such an oxygenated microenvironment around the

tracks of high-LET (24 MeV) carbon ions [135]. They found an increase in the initial track concentration of oxygen, which is in accordance with oxygen in track hypothesis. This was supposed to explain a higher efficiency of cell killing under hypoxic conditions. Thus, despite the contrary underlying mechanisms, both cases can result in a reduced OER. However, additional explanations were proposed, which are either related to intratrack radical recombination or intertrack effects. In the former case, the intratrack recombinations of peroxide and hydroperoxide radicals increases with the LET, thus decreasing the net amount of peroxides available to react with biomolecules [129, 136]. In the latter case intertrack recombinations, possible at high dose rates, are as well assumed to modify the radical yield. However, Ramos-Mendez *et al* [128] performed simulations with Topas-nBio, that showed that recombinations between different tracks (intertrack effects) for proton beams become only relevant in the low LET regime [128, 129]. Further hypotheses include the prevention of repair mechanisms and/or due to damage of related proteins and enzymes, to explain the observed effects exist, but it is far from being completely understood [130–132]. Additional mechanisms, more related to the later biological stages, are attributed to differences in the activation of metabolic, repair and detoxification pathways between normal and cancerous tissue [130]. Therefore, clearly more research is needed. However, in the future MCS will play an important role to test the different models and optimize clinical parameters such as LET and oxygen dependence, beam properties, dose rate, and fractions [128, 131, 137].

3.2.2. Disentangling the type of damage: Scavenging and the chemical environment

To disentangle direct and indirect radiation damage to biomolecules different approaches exist. One option is to perform experiments under different levels of hydration. For example, near ambient pressure XPS (NAP-XPS) was recently applied in combination with TOPAS MCS, to distinguish direct DNA damage, by photons and LEE, from damage by hydroxyl radicals and quasi-direct effects [56]. The exposure of dry DNA to x-rays showed a preferential induction of strand-breaks at the sugar-phosphate backbone, while deoxyribose and nucleobases were less affected. An overall increase of DNA damage was observed under humid atmosphere, and base damage and base release became dominant, even though the number of strand-breaks increased as well. Similar studies were performed by varying hydration yields of plasmid DNA and measuring the SSB and DSB yield in dependence on hydration, which both increased [59]. Another method is to irradiate frozen samples at different degrees of hydration and measure radical or strand-break yields [60, 138]. Especially the investigation of radical formation by electron spin resonance (ESR/EPR) provides deep insight into the chemical modifications occurring in DNA [60, 139]. This allows for trapping of radicals and separating the effects of different species and to obtain detail information on chemical modifications, as summarized by Adhikary *et al* and references therein [60].

An approach involving less complex experimental setups is the selective scavenging of radical species. These scavengers protect biomolecules by interacting with the radical species before they damage DNA [140]. Frequently used hydroxyl radical scavenger are alcohols [62], dimethyl sulfoxide (DMSO) [141, 142], glycerol [143], 2-propanol [64], Tris(hydroxymethyl)aminomethane (Tris) [144, 145], and compatible solutes such as ectoine [146, 147]. To scavenge prehydrated electrons NO_2^- and NO_3^- are applied frequently [107, 148]. When applying these scavengers, their influence on the solvent, the biomolecules themself and the reactivity of the resulting reaction products of the scavenging reaction have to be taken into account [141,144,149–154]. To simulate scavenging capacities of the environment during the chemical stage the mean lifetime of the hydroxyl radical can be modified to represent the effective scavenging capacity of the medium. By this approach Valota *et al* studied the protective effects of radical scavengers following gamma irradiation against SSB and DSB induction in DNA structures ranging from linear DNA, over minichromosomes to chromatin [142]. The recent implementation of the IRT models in Geant4-DNA and TOPAS-nBio provided the option to directly simulate radical scavenging by explicit inclusion of scavengers [124]. Validation of these models was performed by determination of the SSB yield upon gamma radiolysis in plasmid DNA pUC18 dissolved in aerated solutions containing DMSO. They found that an SSB efficiencies of 24% for hydroxyl radicals and 0.5 % H radicals led to the best agreement between experiment and simulations [54]. The work by Dominguez-Kondo *et al* applied the IRT models to simulate SSB and DSB yields for enhanced time scales up to 20 μs in plasmid DNA [155]. This allowed them to successfully reproduced SSB yields as a function of DMSO concentration and showed the feasibility to directly test simulations of the physical and chemical stage against published datasets for plasmid DNA [155], which enables future applications in evaluating currently developed plasmid DNA based biodosimeter, which are being evaluated as a candidate for a future reference material for DNA based biodosimetry [156, 157].

4. The targets of radiation therapy

On the macroscopic scale the target of radiation therapy is the cancerous tissue. Within cells the cellular organelles such as the nucleus or mitochondria are of importance due to their central for the genome and metabolism, respectively [16]. On the molecular level, DNA, proteins and RNA are of interest, due to their overall importance for function and survival of the organisms.

4.1. Biomolecules

Traditionally, most of the radiation related research on the molecular level was targeted towards DNA, which is of key interest due to its central role in reproduction, transcription, mutation and apoptosis [55]. Proteins are much more diverse in structure and function than DNA, more abundant and easier replaceable within a cell. Therefore the greatest focus lies on proteins which interact with DNA and how this interaction modifies DNA related radiation damage [158, 159]. During the Covid-19 pandemic the deactivation of SARS-CoV-2 virus for vaccine development by radiation, the related spike-protein and especially the RNA within gained some interest and was studied by Geant4 MCS [160, 161].

4.1.1. DNA

In isolated DNA molecules the damage can occur at its different building blocks, the sugar-phosphate backbone and the nucleobases. The most relevant types of DNA damage, which can lead to damage of the genome, are SSB and DSB at the sugar-phosphate backbone and base damage or base loss creating an abasic site. SBs are mostly produced by cleavage of the C-O bond of the phosphate backbone, while base releases is related to damage of the N-glycosidic bond [162]. The initial distribution of direct ionization events from high-energy particles at biomolecules correlates with the electron density at the different subgroups [60, 121]. In the case of DNA, an ionization event leads to the ejection of an electron, and produces a hole which can migrate within the DNA. This hole can react at the backbone and lead to a SSB, or it can localize at the nucleobases. Hereby a location preference for guanine was observed [60, 154, 163]. Energy dependent direct damage yields from ionization events caused by electrons between 25 eV to 4 keV for SSB and DSB induction were quantified by Folkard *et al* [164]. As already discussed above in the case of water, vLEEs with energies below 20 eV can form TNI at DNA and cause damage DNA by resonant processes such as DEA or shape resonances. For DNA, it has been shown that direct attachment at the 3- and 5-positions of the carbon atom of the sugar phosphate group is relatively rare. Most of the damage is caused by resonant attachment of the electrons at the free π-orbitals of the nucleobases [112]. This leads either to damage of the respective bases themselves, or to an ET process to the DNA backbone. For example, vLEEs with kinetic energies in the range of 4-16 eV, the SSB yield is approximately two times higher than the yield for base release [165]. Thus, the damage yields of these processes depend strongly on the initial electron capture probability of the DNA nucleobases. Therefore a dependence of strand breaks yield by DEA on base type and sequence can be assumed. In fact, a vacuum study conducted by Solomun *et al* showed an increased DNA damage efficiency for guanine in relation to adenine [166]. However, experimental work on different molecules in ice [167, 168] and theoretical work [112] including water, showed a strong influence of such polar environments on the occurrence and energetic position of the resonances. Many resonances above 1 eV, which are effective in the gas phase, seem to be quenched by the polar environment. In contrast, the effective cross sections of the resonances around 0 eV–1 eV are strongly increased as it was observed by Lu and Sanche [167, 168]. Further details on electron induced damage to DNA can be found in the review by Alizadeh and Sanche [65].

To study these processes by MCS it is necessary to include appropriate electron scattering cross for the nucleobases (adenine, thymine, guanine and cytosine). These were implemented recently for high energy processes such as ionization in Geant4-DNA within a specialized physics constructor (*option6*) providing good agreement with experimental work in the high energy range, while still deviating in the low-energy region, where attachment processes come into play [169, 170]. To improve this situation combined effort of theoreticians and experimentalist is undertaken in evaluating scattering behaviour of model systems such as THF and isolated DNA constituents [87,169–174].

Besides LEE and vLEEs the huge variety of radical species, their reaction rates, diffusional behaviour and varying scavenging capacities of the buffers used, pose difficulties to accurately predict damage outcome. A comprehensive overview about this topic can be found in the books by von Sonntag [61, 62]. Briefly, the most abundant radical species produced by high energy radiation in water are the hydroxyl radical and the (pre) solvated electron.(equation (2)) When ionization processes in water dominate they are approximately produced in a similar ratio [175]. Hereby, the OH radical is highly reactive and can attack unsaturated bonds with quasi-diffusion-controlled rates [55]. Further reactions of the hydroxyl radical with oxygen can lead to a large number of stable end products on DNA. This is related to the oxygen fixation hypothesis, which proposes that oxygen

fixes radical-induced DNA damage, making it permanent. Thus explaining the resulting different radiosensitivity of cells under aerobic and and hypoxic conditions as described by the OER [133]. In total, bases account for about 80% of the damage induced by hydroxyl radicals, which however, can be effectively repaired by cellular mechanisms. The proportion of damage caused by hydroxyl radicals leading to SSB is about 11 % [55]. This is attributed to the reduced reaction rate and to lower accessibility of the H-atoms of the sugar, which are partially shielded by the geometric structure of the double helix in dsDNA [55]. Hydroxyl radicals have long been considered to be the main cause of DNA damage [55, 62, 122, 138, 176]. This is based on the fact that in the presence of water, the number of DNA damage increases by orders of magnitude and thus a dominance of indirect damage mechanisms seems likely [138]. In contrast, experiments conducted in the presence of high concentrations of $^{\bullet}OH$ scavengers showed that only up to 65% of the SSBs and DSBs can be scavenged. So the relative percentage of direct, quasi-direct and indirect damage is still under debate depends not only on radiation properties such as LET, but as well on a multitude of factors, such as pH and scavenging capacity of the buffer, salt, oxygen ((non)hypoxic conditions) and cosolute concentrations, as well as type of DNA (single-stranded (ssDNA) or double-stranded (dsDNA) DNA), DNA density, protein binding, base sequence, geometrical arrangement and others [176]. Additional complexity arises by taking into account the roles of species like H^{+}, e^{-}_{pre} and e^{-}_{hyd}, which can form adducts with biomolecules. The reaction rates of hydrogen radicals are also reduced in comparison to those of hydroxyl radicals [62]. The proportions of SSBs and DSBs induced by the fully solvated e^{-}_{hyd} is relatively small in relation to those of $^{\bullet}OH$ or e^{-}_{pre}. This is attributed to the fact that e^{-}_{hyd} are trapped in a -3 eV deep potential well and and thus have a decreased reactivity (figure 6 right) [3]. However, there are reports that e^{-}_{hyd} has increased reactivity when DNA forms adducts with cisplatin, which is a common chemotherapy medication [177]. For details see below (section 4.4). The efficiency of the short lived prehydrated electron in causing reductive damage to DNA or its components by DET is currently debated, due to observations of different groups varying between the different targets, conditions and techniques applied. For details on this discussion the literature of the different groups is of interest, namely by Lu [64,113,178–180], Abel [111, 120, 181], and Mostafavi [67, 68, 182]. However, to include these effects in a reliable manner in MCS simulations of the physico-chemical stage, clearly more experimental work and data is needed.

Despite these uncertainties with respect to some of the associated processes the predictive power of the models lead to similar damage thresholds between diverse settings. For example, the SSB and DSB yields from direct and indirect radiation effects by Geant4-DNA and the influence particle type and LET was studied by Villagrasa *et al* [183] They concluded that the best agreement with the number of radiation induced DNA damage foci in dependence of LET was achieved, when an energy deposit threshold for SSB induction in the backbone of one nucleotide was set to $E_{SSB} \geqslant 17.5\ eV$. Furthermore, Hahn *et al* studied the SSB induction in pUC19 plasmid DNA by 30 keV electrons in water during a combined experimental and simulational study and determined a median lethal dose as $D_{1/2} = (1.7 \pm 0.3)$ Gy and an SSB to DSB ratio of 12:1 [175]. This work was later extended by incorporating a microscopic target model, based on studies by Lindborg *et al* [12, 21], and an extended set of experimental data and diffusion and particle scattering simulations [4]. By combining experimental and simulational results it was found, that on average less than two ionizations within a target sphere of 7.5nm radius around the sugar-phosphate backbone are sufficient to cause a SSB, with a corresponding median lethal energy deposit being $E_{1/2} = 6 \pm 4$ eV [4]. Furthermore, Liang *et al* [28] compared the RBE with relative DSB induction in simulated chromatin model, between the interaction from ultra soft (278eV-4.5 keV), soft (25 KVp and 55 kVp) and conventional x-rays (>80 keV). Their analysis indicated, in line with experimental evidence, that the formation of complex DSBs are detrimental for the proper function of DNA repair machinery and seems to contribute predominantly to the formation of lethal damage [28].

To facilitate the exchange between simulation results of damage induction in DNA and the modeling of biological DNA repair processes as well as the effects of the environment a new standard DNA damage (SDD) format was proposed by Schuemann *et al* [184] The SDD aims to unify the interface between the simulation of DNA damage and the modeling of DNA repair processes, and introduces environmental effects. To help with the testing of complex DNA geometries, the program *DnaFabric* was developed by Meylan *et al* which provides an accessible way to export DNA models directly into Geant4 [185]. *DnaFabric* allows the user to generate, modify, visualize and simulate multi-scale models of DNA. These models cover different levels of complexity, ranging from the DNA double helix, nucleosomes, hetero-chromatin fibres, chromosomes and their domains, as well as a complete cell nucleus. This allows to include the full content of the human genome with about 6.4×10^{9} nucleotides in a simulation [185]. Furthermore, they extended the default Geant4-DNA chemistry module to implement the reaction of hydroxyl radicals with the DNA constituents, which are characterized by their respective radius, i.e. 0.29 nm for the 2-deoxyribose, 0.27 nm for the phosphate group and 0.3 nm for the nucleobases. The respective reaction rates implemented are (in $10^{-9}\ M^{-1}s^{-1}$): for 2-deoxyribose$+^{\bullet}OH$ (2.5), Adenine$+^{\bullet}OH$ (6.1), Guanine$+^{\bullet}OH$ (9.2), Thymine$+^{\bullet}OH$ (6.4), Cytosine$+^{\bullet}OH$ (6.1) [185]. The resulting indirect DNA is calculated in multiple steps. Following the simulation, the position and volume of the DNA is

superimposed with the locations of the diffusing radicals. After an encounter between a DNA constituent and the $^{\bullet}OH$ radical the outcome can be calculated, by taking into a certain damage probability. For example, Meylan *et al* assumed that an encounter between an $^{\bullet}OH$ radical and either a 2-deoxyribose or a phosphate group would lead with a 40 % probability to a DNA strand-break. In comparison, for direct damage a 17.5 eV threshold for the energy deposited in the backbone of a nucleotide for a SB induction was assumed [185].

Generally, there are many additional reaction pathways with DNA for the different radical species produced during water radiolysis. Furthermore, their reaction with DNA may involve several steps before the biologically relevant endpoint is reached. However, most of them have lower lifetimes and reaction rates than the $^{\bullet}OH$ radical. Inclusion of the related additional DNA-radical reactions in Geant4 is ongoing work [185]. All these processes and their reactivities are discussed in detail by von Sonntag [62].

Within TOPAS-nBio various DNA models are already included by default [15]. A simple cylindrical model for DNA strands, nucleosomes and chromatin based on the work by Nikjoo *et al* [186, 187], the cylindrical model of Charlton *et al* representing bases and backbone [188], and similar linear and circular plasmid DNA models. Furthermore, different models for supercoiled plasmid DNA are available, based either on Vologodskii and Cozzarellis work [189], or the DNA fabric models by Meylan *et al* [185]. A complex solenoid chromatin fiber model including the histone proteins and hydration shell are available as described in the literature [17, 190]. Here it has to be noted that the exact choice of DNA model, the geometry and damage scoring parameters have a huge influence on the outcome of damage yields of direct and indirect effects as it was recently shown in a TOPAS-nBio based study conducted by Bertolet *et al* [190]. They showed that the imprecise geometric models can lead to significant differences in the prediction of damage yields in terms of type of damage and their origin. Another extension called *PDB4DNA* allows to import molecular structures stored in the protein database (PDB) format into Geant4 [46]. It is based on the open-source library PDBlib and can convert PDB description files of DNA or proteins into a Geant4 geometry at the atomic level. Besides visualization PDB4DNA allows to assign simulated energy deposition to individual atoms for predicting direct damage. This allows direct study of complex geometries described in the PDB format such as the different topologies of plasmid DNA [191] which are used in the development of DNA based biodosimetry [156, 157, 192] complex cellular DNA models [193], or structures such as RNA, membranes and proteins [45, 159].

4.1.2. Proteins and DNA-protein complexes

Proteins play a vital role in maintaining cellular function. They are essential during DNA repair. For example, during radiation response and DSB repair in DNA via homologous recombination, single-strand DNA binding proteins (SBPs) promote induction of ssDNA at the sites of the DSB [159]. Currently, little is known about the radiation response of SBPs or SBPs-DNA complexes (SBP-DNA). Neither SBP inactivation dosages nor the nature and modifications of SBP-DNA by radiation are quantified. This contrasts with dsDNA-protein systems, where significant information exists [158, 194]. Many of this knowledge originates from x-ray crystallography for the determination of 3D structures of DNA-protein complexes, which is typically performed at low temperatures (100K), where direct damage by x-rays and secondary electrons dominates [195]. Under this conditions DNA is less radiation sensitive compared to proteins. However, comparability with studies under physiological conditions cannot be assumed *a priori*, due to the damage caused by radical species produced upon water radiolysis. On the other hand, most of the irradiation studies on DNA-protein complexes under physiological conditions focus on direct damage by high energy particles and indirect damage by OH-radicals [158, 194, 196]. There it was found, that protein binding protects DNA against OH-radical attacks via geometry dependent shielding [158], while formation of DNA-protein crosslinks increases [196]. Additionally, protein binding can modify the reactivity of nucleotide radicals by disrupting DNA base stacking [197], and alters the charge migration through the DNA duplex [198–201]. However, these studies do not consider the damage by LEEs and prehydrated electrons. Until today, the influence of bound SBPs on ssDNA damage by LEEs was investigated only *in vacuo*. Thereby, electron irradiation (3 eV) of immobilized DNA oligonucleotides with and without bound SBPs (*E. coli*SSB) was performed [202]. The protective effects of SBPs were explained by density functional theory (DFT) calculations which showed that SBPs modify the lowest unoccupied molecular orbitals of DNA upon binding [202]. Abdoul-Carime and Sanche studied LEE induced anion desorption from dry films of various amino acids and their compounds [203–205]. They found that disulfide bonds are damaged more easily compared to peptide bonds. Additionally cysteine was found to be two orders in magnitude more susceptible to DEA than glycine and alanine. This was attributed to the sulfur group of cysteine [204]. Later, Ptasinska *et al* investigated the damage induced by 1 eV electrons to complexes of the amino acids glycine and arginine with oligonucleotides [206]. For low amounts of glycine, fragmentation of the oligonucleotides increased. This was attributed to the hydrogen radicals produced from glycine. However, for higher concentrations they observed a protective effects by both amino acids. This can be understood by the first-principle molecular dynamics simulations of Gu *et al*[207] and DFT calculations [202, 204]. It was concluded that amino acids can act as protective agents for nucleobases against LEE damage either by scavenging of the

excess electrons, by stabilizing them at the nucleobases [207], or by modification of the lowest unoccupied molecular orbitals of the DNA upon binding [202]. However, these are gas-phase results and the type and yield of damage is expected to change under physiological conditions when DNA and proteins are solvated and radical species are produced by water radiolysis. Similar protective effects were found in a simulational study for histones which were shown to influence the interaction of electrons with DNA [208]. In a recent work by Hallier *et al*[159] small-angle x-ray scattering (SAXS) at the SBP *gene 5 protein* (G5P) [18, 209] were combined with TOPAS-nBio simulations to determine the microscopic energy deposit-damage relation for G5P. The median energy deposit within its target volume for the induction of structural changes of G5P was determined as 7 ± 5 eV. Whereby the presence of the scavenger ectoine increased the possible exposure time before radiation induced structural changes were observed [159]. In the same work a related TOPAS-nBio extension to estimate the microscopic dose received by biomolecules during bioSAXS experiments was made available [210]. More complex DNA-protein compounds, i.e. chromatin, are found in the nucleus of mammalian cells. They were studied by Tang *et al* in the form of heterochromatin and euchromatin [211]. The analysis of their simulations revealed more direct damage induction and less indirect damage in heterochromatin than in euchromatin after irradiation with protons and alpha particles. Still, the complexity of the DSB was similar in both targets, heterochromatin and euchromatin models. An additional topic of importance related to protein interaction with radiation is the formation of covalent DNA-protein crosslinks. This is due to the fact that they are predominantly formed under low oxygen concentrations which occur in cancerous tissue with high radiation resistance [212]. Despite the importance of the underlying mechanism for treating these tumors, only some studies use MCS based simulations to study the related mechanism, focusing on Geant4 aided dosimetry [213].

4.2. Cells and their organelles

Besides the nucleus of mammalian cells, other parts of the cell, the organelles such as mitochondria, or the membrane are integral part of the cells to maintain their function and integrity. However, the complex chemical environment with many cosolutes, differing scavenging capacities, and intermolecular interactions can modify the outcome substantially [121]. Therefore detailed models of the cells and their organelles are needed which incorporate the specific geometrical constrains of the DNA and DNA-protein complexes within. A complete nucleus model is already provided by TOPAS-nBio [214]. Within the nucleus of the form of a ellipsoid the whole human genome with about six Giga-basepairs can be modeled over different structural levels, as chromatins, nucleosomes including histones, and dsDNA strands. During a study performed by Gonon *et al* different models of nuclei were benchmarked by comparison with experimental yields of DNA damage after irradiation with an ion microbeam [215]. Their comparison of the results showed an increase of relative frequencies of foci/simulated DNA damage in the nuclei of the cells with increasing LET until they reached quasi-plateau for LET values above 80 $keV/\mu m$. A methodology to develop realistic mitochondria models based on microscopy data for Geant4 was described in the work by Zein *et al* [216]. This goes beyond the approximation often used for simple simulations of the mitochondria as ellipsoid without taking a more detailed structure into account. In TOPAS-nBio a range of cell models are included, from simple geometry derived shapes such as, spheres, ellipsoids and cubical cells, models for irregular shaped fibroblast, bone cells in the form of osteocytes and osteoblasts, as well as red blood cells, and white blood cells in the form of basophils, eosinophils, lymphocytes and monocytes [45]. Their specifica and parameter can be found in the TOPAS-nBio documentation [15]. Furthermore different neuron and glial geometries can be included by loading cell definitions in the *SWC* format. Most of these models offer the inclusion of a nucleus and other organelles such as mitochondria. Recently, a cell model was extended to include additional substructures to include a cell membrane as separate target and nanoparticles for the simulation of their effects as radiosensitizer (figure 1), details can be found in section 4.4 [16, 217]. Such cell models can be used for complete simulation of the physical, physicochemical and chemical stage. A study of early radiation damage by protons at the scale of at fibroblast with Geant4-DNA was performed by Meylan *et al* [185].Beyond isolated cells, TOPAS-nBio includes a structure to simulate cell cultures to model, for example, irradiated petri dishes (figure 1 center). The complex interaction between cells and radiation induced signalling processes are even more difficult to study. Hereby a prime example is the radiation-induced bystander effect [218]. Their term refers to cells which die or show choromosomal instability without having been directly irradiated during a treatment, as observed by Nagasawa and Little [219] after subjecting Chinese hamster ovary cells (CHO) to low doses of alpha particles, or by Sedelnikova *et al* which found DSB in bystander cells after irradiation of a human tissue models by a microbeam [220]. To study these effects with a multi-scale approach Geant4 and *CompuCell3D* [221] were combined by Liu *et al* via a newly developed bridging module named *RADCELL* [222]. This allowed them to combined simulations of cell biology and particle-scattering simulations to study and quantifying cell behavior after irradiation. As a proof of concept they simulated as vascular tumor and produced a range of biologically reasonable morphologies which are intended to study growth rate, size, and morphology of the tumor. Their method allows for quantitative studies of

radiation damage in cells, with the long-term goal to study radiation response on the tissue level. Another project which was recently proposed and is currently under development is the *MIcrodosimetry and NAnodosimetry to Simulate The Initial Radiation-Induced damage Topologys Heterogeneity* (MINAS TIRITH), which is a Geant4-DNA based tool to model radiation damage at the cell population scale which was recently described [223].

4.3. DNA repair mechanisms

After irradiation various cellular repair mechanisms take place to detect and repair DNA damage. The implementation of these processes is needed to cover the whole range of processes and predict the outcome of irradiation experiments *in-vivo*. Within the last years, different groups started to implement the most relevant repair processes in Geant4-DNA and TOPAS-nBio [17, 41, 145–224, 227]. For example, extensions for TOPAS-nBio allow for modeling of biological DNA repair processes and cell survival. *DaMaRiS* (DNA Mechanistic Repair Simulator) from the University of Manchester allows to simulate non-homologous end Joining (NHEJ) based on an initial DNA damage distribution [17, 224–226]. Such a DNA distribution can be provided by the SDD format as described above [184]. DaMaRiS can be directly accessed from TOPAS-nBio itself and allows therefore for a coherent workflow. Another tool to simulate cell survival and incorporate DNA repair is *MEDRAS* (Mechanistic DNA Repair And Survival), which was developed at Queens University in Belfast [41, 227]. Here, an initial distribution of DNA damage is the starting point to model the location dependent and constrained interactions of DSB ends. From this data correct end joining and misrepair is simulated. In this process the repair kinetics of the three major repair processes, NHEJ, homologous-recombination (HR) and micro-homology mediated end joining (MMEJ), are considered. This allows for estimation of different biological endpoints, including DSB repair, misrepair, induction of mutation and chromosome aberration and cell survival. A very recent publication presented a Geant4-DNA extension implementing a feature for the prediction of DNA rejoining kinetics and cell survival in time after irradiation for a Chinese hamster V79 cell line [228]. There the two lesion kinetics (TLK) model was implemented and successfully applied together with an optimized parameter set to predict DNA repair kinetics and cell survival. Furthermore, the recently described MINAS TIRITH is planned to be connected with repair models, especially for the case of the kinetic modeling of foci, to approach real world experimental conditions [223].

4.4. Radiosensitizer

To increase the local energy deposit in cancerous tissue various radio-sensitizing therapeutics such as metallic or metal oxide (high-atomic number/high-Z) nanoparticles, cisplatin and halogenated nucleotides are evaluated and employed [229–232]. To increase their efficiency, a better understanding of the underlying sensitizing mechanisms is necessary [66, 233]. This radiosensitization by metallic nanoparticles is caused by their higher electron density compared to the solvent and biomolecules, which leads to an increase of the local scattering cross section and an increased production of damaging species such as LEEs, Auger electrons, and ROS [231, 234, 235]. Besides, plasmon excitation in metallic nanoparticles can function as an additional source of LEE [236, 237]. To apply them successfully during radiation therapy, their energy deposit characteristics and possible dose enhancements and biological effectiveness in dependence on their intracellular location have to be studied [16, 232, 234, 238, 239]. Thereby the physical action itself, the dose enhancement factor (DEF) in dependence of size, particle density and their position within the cell, the induced ROS production and heat transfer, as well as influence on biological functions of the cell are variables to be considered. This characteristics depend on many factors such as nanoparticle material, size and possible surface functionalization, their cellular uptake and interaction with the type of radiation used [16, 234, 235, 240, 241]. For example, the prerequisite to determine realistic DER by MCS was recently studied by Rabus *et al*, and the importance of fulfilling the condition of having a secondary particle equilibrium during MCS was pointed out [239].

Currently, many nanoparticle related studies focus on gold nanoparticles (AuNPs) This is due to the fact that cellular uptake of AuNPs takes place for diameters up to some tens of nanometers [242]. They are evaluated for different types of therapies, such as external beam therapy [243, 244], in brachytherapy [245], for photothermal therapy in combination with pulsed laser sources [231, 246], and as radioactive nanoparticles [234,247–250]. To obtain a detailed understanding of the radiosensitizing mechanisms, the kinetic energy spectrum of secondary particles emitted from the nanoparticle surface and the spatially resolved energy deposit have to be studied. For the case of AuNP a Geant4 based study was performed and energy deposit characteristic in dependence on size and clustering behavior was reported by Zutta *et al* [234]. The same authors developed a TOPAS-nBio based extension to study cells in combination with randomly distributed nanoparticles in the cytosol and organelle targeting nanoparticles which are described in detail in their later work (compare figure 1 center) [16]. Tran *et al* performed the first Geant4 based MCS with protons in the energy range of relevance for clinical proton therapy (2-70 MeV) and determined DER and related radiolysis enhancement factor (REF) related to the chemical stage. The main effect determining the DER and REF values were related to additional LEE production from the

interaction between AuNP and the protons [235]. To obtain accurate results it is of importance to perform nanoparticle related simulations with track-structure based code which enables step-by-step simulations of the scattering interaction. The explicit simulation of every step provides higher accuracy than the faster, condensed-history codes [251]. Therefore it is recommended whenever available, to apply explicit scattering models for the nanoparticle material in use. For example, in the case of gold there were implemented by Sakata *et al* [251–253]. Furthermore the material specific scattering models which for processes such as atomic de-excitation, Auger electron emission, Auger cascade and fluorescence emission have to be activated [254, 255]. Currently ongoing work is performed by Rabus and coworkers to provide experimental reference data for benchmarking MCS simulated radiation effects of gold nanoparticles [256, 257]. An extension of these experimental and simulational efforts, currently being undertaken for AuNP, to other metallic nanoparticles, would be of great interest to the community.

The enhanced track structure models for gold were applied by Engels *et al* to study the effects of AuNP on a clinical x-ray beam [232]. The simulation results were related to *in-vitro* brain cancer cell survival curves with a local effect model. The comparison showed that the simulations and local effect model can be used successfully to predict cell survival for the x-ray beam used. Klapproth *et al* performed multiscale MCS of AuNP enhanced DNA damage by x-rays in an xenograft mouse model [258]. They applied phase spaces to perform the transfer from the macroscale cell model to the microscale DNA model. The results showed a damage dependence on cell position within the tumor and and sensitizing effects of the different AuNP studied. Further details on applications and challenges for metallic nanoparticles in radiation therapy are provided in the recent review by Schuemann *et al* [259].

In contrast to metallic nanoparticles cisplatin and halogenated nucleotides are primarily used as chemotherapeutic agents [231]. Both are interfering with the cell cycle due to their influence on DNA replication. This is either achieved by adduct formation between cisplatin and DNA [177] or by incorporation of the halogenated nucleotides [260]. Additionally to this chemotherapeutic effects, additional radiosensitizing was reported beyond similar addition of chemotherapeutic and radiation therapy effects ascribed alone [231, 261]. The halogenated nucleotides are thought to dissociate upon interaction with electrons and form halogen based radical species, which in turn cause DNA damage. Cisplatin forms adducts with guanine rich DNA sequences and is assumed to modify electron structure and related DEA and ET probabilities. Due to their action on the molecular scale, less MCS based studies are present in the literature with respect to cisplatin. Hereby the study by López-Laurrabaquio *et al* [262] used TOPAS-nBio to analyse ROS yields from secondary and Auger electrons scattering with cisplatin, while Baulin *et al* [263] quantified DEF from cisplatin interaction under x-ray irradiation. Furthermore, for appropriate MCS based studies of halogenated nucleotides future extensions of the simulation toolkits would need to incorporate related scattering cross sections and chemical reaction pathways for the involved molecular groups.

5. Summary and conclusion

Geant4 based MCS have come a long way from their origins in high-energy physics [34, 35]. They have been extended successfully towards low-energy interactions in water [36, 37], and to simulations of the chemical stage including the subsequent production, reactions and diffusion of ROS [39, 40]. Beyond the physical and chemical stage, the prediction of DNA damage and repair processes can be simulated nowadays for users without expert knowledge in *C++* with TOPAS-nBio [15, 17, 41].

However, there are still many areas where improvements are needed to increase accuracy, accessibility and predictive power. On the fundamental level, there is a need to improve the accuracy of LEE scattering cross-sections in water, since these are not based on data from liquid water but on measurements at amorphous ice [116, 117, 264]. Here, applying advanced experimental techniques, based on liquid-jet technology [265, 266], differential pumping setups in vacuum environments [56, 267], or nano-membranes [175, 268], might provide as solution to the experimental challenges occurring, when LEE interaction with liquid water have to be studied. Similarly, the accurate cross sections for direct interaction of radiation with different parts of DNA, or materials evaluated as radiosensitizer are needed [87, 171]. For DNA this is further complicated by the dependence of its radiation sensitivity on the local environment, e.g. ionic strength, base-pairing or presence of oxygen or cosolutes [27, 61, 147]. For materials used in radiosensitizers specific excited states and nanoparticles size dependent effects, such as plasmon excitations, may become important in the low-energy range for ultraviolet or optical photons and LEE [252, 256]. The simulation of the chemical stage is still a computationally demanding task. Even though the situation improved somewhat with the introduction of the IRT, it is expected to benefit from optimized use of multithreading in the future [124]. Furthermore, the complexity originating from the many possible reaction pathways and the scavenging capacity within a realistic cellular environment in dependence of cell type, cell cycle, oxygen content, and dose-rate dependent factors, highlight the need for

additional experimental data to improve the overall modelling [128, 176]. The aspect of dose-rate is of special importance for a promising development in therapeutical approaches, which make use of the FLASH effect to decrease the radiation toxicity while achieving the same tumor control [137, 269]. Due to the high-dose rates the possibility of intertrack reactions during the chemical stage increases and leads to altered complex chemical behaviour and new reaction pathways [129]. Similarly, the modelling of DNA damage and repair processes involve many assumptions and simplifications. Here, the simulations may benefit from more realistic models for SSB induction which often only depend on local energy deposit [4, 227]. For the estimation of the effects of DSB the inclusions of different types of complexity of the DSB and their consequences for repair kinetics have to be considered as well [17, 227]. Wider adaption of the SDD format will help to compare simulational results and analyse them in a coherent manner [184]. The availability of ready to use cellular models makes the study of different cell lines more accessible and in increase comparability of related results as well [15, 16, 45]. Hereby the prediction of cell-survival is the benchmark for testing new models [232]. Going beyond isolated cells to study phenomena such as the radiation induced bystander effect [222] or the radiation response on a tissue level [223] are still in an early stage. However, complete multiscale models including AuNP radiosensitization of DNA into a xenograft mouse model highlight already what can be achieved by integration and combination of simulation and modelling techniques on different scales [258]. Thus, important first steps and proof of concepts were successfully delivered and will be extended and applied to a broader range of conditions during ongoing and future work [222, 223].

In summary, despite many open questions and the need to further improve basic cross-sectional data and damage models, MCS-based methods have already demonstrated their predictive power in successfully modeling DNA damage of varying complexity, as well as cellular radiation response and survival under different conditions. In particular, the successful multiscale approaches linking fundamental damage mechanisms from scattering events at the atomic level to chromosome damage, DNA repair processes, and survival or apoptosis highlight the power of current simulation frameworks and their extensions. When these models and simulations are combined with experimental data, an understanding of the underlying mechanisms of radiation damage to tissue is achieved that is difficult to obtain using experimental or computational techniques alone. Based on this understanding, more efficient and targeted radiation therapies to cure cancer will be developed.

Acknowledgments

Discussions with Dr. Tihomir Solomun and Dr. Robin Schürmann, as well as support with CAD visualization by Sven Fritzsche are gratefully acknowledged. This work was funded by the Deutsche Forschungsgemeinschaft (DFG, German Research Foundation) under grant number 442240902 (HA 8528/2-1).

Data availability statement

No new data were created or analysed in this study.

Competing interests

The authors declare that they have no competing interests.

ORCID iDs

Marc Benjamin Hahn https://orcid.org/0000-0002-5050-7083

References

[1] Simmons J A and Watt D E 1999 *Radiation Protection Dosimetry: A Radical Reappraisal* (Madison, Wis.: Medical Physics Publishing)
[2] Solov'yov A V (ed) 2017 *Nanoscale Insights into Ion-Beam Cancer Therapy* (Cham: Springer International Publishing)
[3] Alizadeh E and Sanche L 2012 *Chem. Rev.* **112** 5578–602
[4] Hahn M B, Meyer S, Kunte H J, Solomun T and Sturm H 2017 *Phys. Rev.* **95** (5) 052419 E
[5] Kellerer A M 1985 Fundamentals of microdosimetry *The Dosimetry of Ionizing Radiation* ed K R Kase, B E Bjärngard and F H Attix (Academic Press) pp 77–162
[6] Rossi H H and Zaider D M 1996 *Theoretical Microdosimetry Microdosimetry and Its Applications* (Berlin Heidelberg: Springer) pp 148–204
[7] Goodhead D T 2006 *Radiat. Prot. Dosim.* **122** 3–15
[8] Grosswendt B, Pszona S and Bantsar A 2007 *Radiat. Prot. Dosim.* **126** 432–44
[9] Solov'yov A V, Surdutovich E, Scifoni E, Mishustin I and Greiner W 2009 *Phys. Rev.* E **79** 011909

[10] Palmans H *et al* 2014 *The British Journal of Radiology* **88** 20140392
[11] Goodhead D T 2015 *Radiat. Prot. Dosim.* **166** 276–81
[12] Lindborg L, Hultqvist M, Tedgren Å C and Nikjoo H 2015 *Radiat. Prot. Dosim.* **166** 339–42
[13] 3D Printable David by Scan The World https://www.myminifactory.com/object/3d-print-michelangelo-s-david-in-florence-italy-2052
[14] Thingiversecom Human Brain, Full Scale by MiloMihttps://www.thingiverse.com/thing:371899
[15] Schuemann J, McNamara A L, Ramos-Méndez J, Perl J, Held K D, Paganetti H, Incerti S and Faddegon B 2019 *Radiat. Res.* **191** 125–38
[16] Hahn M B and Zutta Villate J M 2021 *Sci. Rep.* **11** 6721
[17] Henthorn N T, Warmenhoven J W, Sotiropoulos M, Mackay R I, Kirkby K J and Merchant M J 2017 *Radiat. Res.* **188** 770–83
[18] Hahn M B *et al* 2015 Influence of the Compatible Solute Ectoine on the Local Water Structure: Implications for the Binding of the Protein G5P to DNA *J. Phys. Chem.* **119** (49) 15212–20 B
[19] Perl J, Shin J, Schumann J, Faddegon B and Paganetti H 2012 *Med. Phys.* **39** 6818–37
[20] Kellerer A M 2004 *Radiat. Prot. Dosim.* **110** 781–7
[21] Lindborg L, Hultqvist M, Tedgren Å C and Nikjoo H 2013 *Phys. Med. Biol.* **58** 3089
[22] IAEA 2008 Relative biological effectiveness in ion beam therapy *Technical Reports Series no 461* (International Atomic Energy Agency)
[23] McMahon S J 2018 *Phys. Med. Bio.* **64** 01TR01
[24] Kellerer A M and Rossi H H 1978 *Radiat. Res.* **75** 471–88
[25] Conte V, Selva A, Colautti P, Hilgers G, Rabus H, Bantsar A, Pietrzak M and Pszona S 2018 *Radiat. Prot. Dosim.* **180** 150–6
[26] Harrison R M, Ainsbury E, Alves J, Bottollier-Depois J F, Breustedt B, Caresana M, Clairand I, Fantuzzi E, Fattibene P and Gilvin P 2021 *Radiat. Prot. Dosim.* **194** 42–56
[27] Ward J F 1994 *Int. J. Radiat. Biol.* **66** 427–32
[28] Liang Y, Fu Q, Wang X, Liu F, Yang G, Luo C, Ouyang Q and Wang Y 2017 *Phys. Med. Bio.* **62** 2153
[29] Lea D E 1962 *Actions of Radiations on Living Cells* II edn (Cambridge University Press)
[30] Friedland W, Jacob P, Paretzke H G and Stork T 1998 *Radiat. Res.* **150** 170–82
[31] Ferrari A, Sala P R, Fasso A and Ranft J 2005 *FLUKA: A Multi-Particle Transport Code*Tech. Rep. SLAC-R-773SLAC National Accelerator Lab., Menlo Park, CA (United States) (https://doi.org/10.2172/877507)
[32] Nikjoo H, Goodhead D T, O'Neill P and Terrissol P 1997 *Int. J. Radiat. Biol.* **71** 467–83
[33] Solov'yov I A, Yakubovich A V, Nikolaev P V, Volkovets I and Solov'yov A V 2012 *J. Comput. Chem.* **33** 2412–39
[34] Agostinelli S *et al* 2003 *Nucl. Instrum. Methods Phys. Res., Sect. A* **506** 250–303
[35] Allison J *et al* 2016 *Nucl. Instrum. Methods Phys. Res., Sect. A* **835** 186–225
[36] Incerti S *et al* 2010 *Med. Phys.* **37** 4692–708
[37] Bernal M A *et al* 2015 *Physica Med.* **31** 861–74
[38] Incerti S *et al* 2014 *Nucl. Instrum. Methods Phys. Res., Sect. B* **333** 92–8
[39] Karamitros M *et al* 2014 *J. Comput. Phys.* **274** 841–82
[40] Ramos-Méndez J, Perl J, Schuemann J, McNamara A, Paganetti H and Faddegon B 2018 *Phys. Med. Bio.* **63** 105014
[41] McMahon S J, Schuemann J, Paganetti H and Prise K M 2016 *Sci. Rep.* **6** 33290
[42] Chauvie S, Francis Z, Guatelli S, Incerti S, Mascialino B, Moretto P, Nieminen P and Pia M G 2007 *Nuclear Science, IEEE Transactions on* **54** 2619–28
[43] Kyriakou I, Emfietzoglou D, Ivanchenko V, Bordage M C, Guatelli S, Lazarakis P, Tran H N and Incerti S 2017 *J. Appl. Phys.* **122** 024303
[44] Poole C M, Cornelius I, Trapp J V and Langton C M 2012 A CAD interface for GEANT4. *Australas Phys Eng Sci Med* **35** 329–34
[257] Borbinha J, Rosales L d l F, Hepperle P, Nettelbeck H, Baek W Y, Di Maria S and Rabus H 2022 Experimental benchmark data for Monte Carlo simulated radiation effects of gold nanoparticles. Part II: Comparison of measured and simulated electron spectra from gold nanofoils arXiv:2212.07367
[258] Klapproth A P, Schuemann J, Stangl S, Xie T, Li W B and Multhoff G 2021 *Cancer Nanotechnol.* **12** 27
[259] Schuemann J *et al* 2020 *Physics in Medicine & Biology* **65** 21RM02
[260] Schürmann R, Tsering T, Tanzer K, Denifl S, Kumar S V K and Bald I 2017 *Angew. Chem. Int. Ed.* **56** 10952–5
[261] Seiwert T Y, Salama J K and Vokes E E 2007 *Nature Clinical Practice. Oncology* **4** 86–100
[262] Lopez-Laurrabaquio G, Cruz-Galindo H S, y Rodriguez M M, Carrizales J M M, Kondo J N D and Martinez M P C 2020 *Revista Mexicana de Física* **66** 797–802
[263] Baulin A A, Sukhikh L G and Sukhikh E S 2020 *J. Instrum.* **15** C06061
[264] Liljequist D, Liamsuwan T and Nikjoo H 2012 *Int. J. Radiat. Biol.* **88** 29–37
[265] Thürmer S, Seidel R, Faubel M, Eberhardt W, Hemminger J C, Bradforth S E and Winter B 2013 *Phys. Rev. Lett.* **111** 173005
[266] Winter B and Faubel M 2006 *Chem. Rev.* **106** 1176–211
[267] Shah D, Patel D I, Bahr S, Dietrich P, Meyer M, Thißen A and Linford M R 2019 *Surf. Sci. Spectra* **26** 024003
[268] Solomun T and Sturm H 2007 *The Journal of Physical Chemistry* B **111** 10636–8
[269] Favaudon V *et al* 2014 *Sci. Transl. Med.* **6** 245ra93